Chemical Engineering Journal 498 (2024) 154468

Contents lists available at ScienceDirect

Chemical Engineering Journal

journal homepage: www.elsevier.com/locate/cej

Enhanced selective extraction of indium and gallium using mesoporous sorbents

Iryna Protsak [a,*], Martin Stockhausen [b], Aaron Brewer [a], Martin Owton [c], Thilo Hofmann [b], Freddy Kleitz [a,*]

[a] Department of Functional Materials and Catalysis, Faculty of Chemistry, University of Vienna, Währinger Straße 42, 1090 Vienna, Austria
[b] Department for Environmental Geosciences, Centre for Microbiology and Environmental Systems Science, University of Vienna, Josef-Holaubek-Platz 2, 1090 Vienna, Austria
[c] Independent Scholar, Surrey, UK

ARTICLE INFO

Keywords:
Gallium
Indium
Critical materials
Sustainable recovery
Mesoporous sorbents

ABSTRACT

Gallium (Ga) and indium (In) are essential elements in numerous industries, most notably in the rapidly evolving field of optical electronics. Due to their scarcity in natural resources coupled with escalating demand, there is an urgent need to develop sustainable technologies for extracting these elements from secondary sources. This study presents the innovative application of two highly efficient sorbents, namely mesoporous silica (SBA-15) and ligand-modified mesoporous silica, for the selective extraction of critical elements like indium and gallium from various multi-element solutions. The SBA-15 sorbent showcased remarkable efficiency in adsorbing gallium at a pH of 3, achieving an excellent adsorption capacity of approximately 90 mg/g, which surpasses previously reported values. Conversely, the ligand-modified silica demonstrated significant effectiveness in extracting indium, with an adsorption capacity of ~ 32 mg/g at pH 3. Furthermore, SBA-15 exhibited remarkable selectivity for gallium in solutions containing Ga, In, and Zn, thereby significantly enhancing the possible recovery of Ga from In/Ga/ZnO semiconductor targets. Additionally, the sorbent displayed exceptional separation efficiency between Ga and Al as well as Ga and In. Similarly, ligand-modified silica showed high selectivity for indium in solutions containing Ga, In, and Zn, achieving excellent separation between In and Zn. Moreover, it effectively extracted indium in binary solutions of In and Sn ions, thereby advancing the recovery of indium from ITO (indium tin oxide) films. After ten cycles of reuse, the sorbents maintained their adsorption capacities, underscoring their potential for industrial applications.

1. Introduction

Technological advancement has spurred rapid growth across various industrial sectors, creating a heightened demand for critical elements such as indium and gallium. Consequently, gallium was classified as a critical material (CM) by the European Commission in 2023, recognizing its crucial role in advanced technological applications [1]. Indium was similarly classified as a CM in previous years [2–4]. Indium is primarily used in the production of indium tin oxide (ITO) [5–7] which is utilized in the manufacturing of liquid crystal displays (LCDs), touch screens, and flat-screen TVs, and it is also employed in solar panels and photovoltaic devices [8–11]. Gallium is today widely used in the manufacturing of semiconductors, light-emitting diodes (LEDs), photodetectors, solar cells, and medical devices [8,11–13]. Indium and gallium are found in the Earth's crust only at low concentrations, with indium occurring at approximately 0.05 ppm and 0.072 ppm in the continental and oceanic crusts respectively [5], while gallium lacks primary ores and is found in trace amounts in mineral like bauxite [13,14]. Indium is primarily obtained as a by-product of zinc mining [5,15], while gallium is typically extracted from aluminum and zinc refining processes [13,16]. The scarcity of these metals in primary resources, coupled with their widespread industrial utilization, underlines the need to develop highly efficient methodologies for their sustainable recovery from secondary sources, including electronic waste, industrial wastewater, and by-products arising from zinc and aluminum production (mineral industrial processing) [5,17,18].

* Corresponding authors at: Department of Functional Materials and Catalysis, Faculty of Chemistry, University of Vienna, Währinger Straße 42, 1090 Vienna, Austria.
E-mail addresses: iryna.protsak@univie.ac.at (I. Protsak), freddy.kleitz@univie.ac.at (F. Kleitz).

https://doi.org/10.1016/j.cej.2024.154468
Received 10 June 2024; Received in revised form 27 July 2024; Accepted 31 July 2024
Available online 2 August 2024

Solid-phase extraction (SPE) is an important technique for metal recovery, employing solid adsorbents to selectively capture target components from aqueous solutions through adsorption, which typically requires at most minimal amount of hazardous organic solvents, unlike conventional liquid − liquid extraction methods [5,6,19–21]. Moreover, compared to liquid − liquid extraction (LLE), SPE offers a straightforward separation process and lower energy consumption. However, there is still limited literature covering the extraction of these metals using SPE sorbents. Among those investigated are resins [22], clays [23,24], some carbon-based materials [12,25–28] and 3D hierarchical β-FeOOH nanoparticles [29].

Silica materials, especially those of the SBA-15 type, whether in their pristine form or surface-modified, remain relatively underexplored for the recovery of these critical metals, even though they exhibit a high surface area, relatively large pores [30], and a range of silanol groups known to be effective in coordinating small ions [20]. The uniform and precisely defined mesoporous channels within SBA-15 ensure enhanced accessibility to active sites, a critical factor in catalysis and adsorption processes. Furthermore, the morphology and particle size can be finely adjusted [31], and the material is amenable to forming monolithic structures, crucial for future industrial-scale sorbent applications [32,33]. Silica surfaces can also be easily functionalized with organic ligands, potentially enhancing the selectivity towards certain ions, unlike carbon-based materials, which lack targeted functional groups for facile functionalization. This deficiency requires additional chemical functionalization steps, which often incur extra expenses and are time-consuming.

In this study, both non-modified and ligand-modified SBA-15 were employed as efficient sorbents for the effective recovery of Ga and In from realistic model solutions based on the composition of semiconductor feedstock targets, including the indium tin oxide elements and others. The modification process of SBA-15 entailed the reaction of aminated SBA-15 silica with the reactive pyromellitic dianhydride (PMDA) via a ring-opening reaction [34], thereby introducing carboxyl groups onto the silica surface and within the pores. These groups act as excellent sorption sites for metal ions [19,35,36]. The respective anhydride was previously utilized as a chelating ligand for designing a selective sorbent aimed at extracting radioactive Th, U, and *non*-radioactive Sc [37]. The respective SPE sorbent has proven to be exceptionally effective in separating Sc from complex multi-element solutions, confirming its sensitivity towards smaller ions. In the present study, PMDA has been employed to synthesize a sorbent for the recovery of Ga and In ions, which share similar ionic charges as Sc ion.

The adsorption properties of the two sorbents, with and without PMDA functionalization, for Ga and In ions were comprehensively evaluated, which involved assessing their adsorption capacities across different concentration ranges, studying kinetics, and conducting selectivity tests with competing elements for each element. Given the significant utilization of Ga and In in solar cells [8,38], selectivity tests were conducted in binary solutions containing different concentrations of these elements. Moreover, since Ga and In are commonly employed alongside Zn in the semiconductor industry [39–41], this study investigated the adsorption abilities of both sorbents in solutions containing these three elements at certain ratios. Considering the coexistence of Ga with Al in waste streams derived from the aluminum production industry [42], the selectivity profile for Ga in the presence of Al was also examined. Finally, the sorbents were tested for their extraction capabilities of In in the presence of Sn, given their widespread use in tin oxide films for electronics production [5]. Exhibiting excellent recovery, good separation factors, and reusability, the sorbents prove to be promising for industrial applications.

2. Experimental

2.1. Materials and methods

Tetraethyl orthosilicate (TEOS, 98 %), anhydrous toluene (99.8 %), anhydrous tetrahydrofuran (99.5 %, THF), poly(ethylene glycol)-block-poly(propylene glycol)-block-poly(−ethylene glycol) (Pluronic P123, $EO_{20}PO_{70}EO_{20}$, $M_n \sim 5800$), sodium hydroxide (NaOH, 98 %) flakes were purchased from Sigma Aldrich. Technical grade ethanol (C_2H_5OH, 96 %) was purchased from Brenntag Austria GmbH. 3-Aminopropyltriethoxysilane (APTES, 98 %), and triethylamine (TEA, 99 %) were purchased from Alfa Aesar. Hydrochloric acid (HCl, 37 %) was purchased from VWR Chemicals. Pyromellitic dianhydride (PMDA, 97 %) was purchased from Fluorochem Ltd. Super pure nitic acid (HNO_3, 67–70 %) was purchased from Carl Roth. Gallium (1000 ppm) and indium (1000 ppm) stocks were purchased from LabKings. Zinc (1000 ppm) and Sn (1000 ppm) stocks were purchased from Inorganic Ventures. Aqueous aluminum (10 000 ppm) was purchased from Fischer Scientific.

Low-angle powder X-ray diffraction (PXRD) patterns were recorded on a PANalytical Empyrean diffractometer (Malvern PANalytical, United Kingdom) in transmission geometry (Focusing mirror) using Cu Kα1 + 2 radiation operated at a voltage of 45 kV, a tube current of 40 mA and with a fixed divergence slit of 0.76 mm. Measurements were performed in the continuous mode with a step size of 2θ of 0.013° and a data collection time per step of 50 s for the transmission mode.

Transmission electron microscopy (TEM) images were acquired using a FEI/TFS Tecnai G2 F20 FEGTEM operating at an accelerating voltage of 200 kV. Sample preparation for TEM imaging involved depositing a small quantity of ethanol containing suspended powder onto a holey carbon film-coated 300 mesh copper grid.

Solid-state nuclear magnetic resonance (NMR) spectra were acquired on a Bruker Avance NEO 500 wide bore system (Bruker BioSpin, Ettlingen, Germany) using a 4 mm triple resonance magic angle spinning (MAS) probe with a resonance frequency of 125.78 MHz for ^{13}C and 99.38 MHz for ^{29}Si, respectively. For ^{13}C, the magic angle spinning (MAS) rotor spinning speed was set to 14 kHz, and the cross-polarization (CP) contact time to 3 ms, while for ^{29}Si, the settings were 8 kHz and 5 ms, respectively. A ramped contact pulse was applied for CP, and during acquisition, 1H was high-power decoupled using SPINAL with 64 phase permutations. Chemical shifts are reported in ppm and referenced externally; for ^{13}C to adamantane by setting the low field signal to 38.48 ppm, and for ^{29}Si to DSS by setting the signal to 0 ppm.

Organic elemental analysis was carried out using an EA3000 CHNS-O elemental analyzer (Eurovector). Each reported value represents the average of three replicate measurements, demonstrating excellent reproducibility.

Thermogravimetric analysis (TGA) was performed on a Netzsch instrument (NETZSCH STA 449F3) from 25 to 800 °C at a heating rate of 10 °C min^{-1} under an O_2/N_2 atmosphere. The mass losses (%) were estimated in the temperature range from 150 to 800 °C.

N_2-physisorption isotherm measurements were conducted at − 196 °C using an Autosorb-$_iQ_2$ sorption analyzer (Anton Paar, Boynton Beach, FL, USA). Prior to measurement, all samples underwent degassing under vacuum at 150 °C for 14 h. The specific surface area was determined using the Brunauer-Emmet-Teller (BET) method within the relative pressure range of 0.05–0.3P/P_o. Pore size distribution plots were generated from the equilibrium branch of the isotherms using the NLDFT method (for silica with cylindrical pore geometry). Data were treated using the ASiQwin 5.21 software provided by Anton Paar Quantatech Inc.

Zeta-potential measurements were performed using a Malvern Nano Zetasizer ZS instrument. Prior to measurements, calibration was ensured by employing a standard suspension containing carboxylate-modified polystyrene latex microspheres with a zeta potential of −40 (±6) mV. Aqueous suspensions of the materials were prepared at a concentration of 0.7 mg·mL^{-1} using ultrasonic bath treatment for 45 min, and zeta-

potential values were determined by analyzing the supernatants.

Inductively Coupled Plasma Optical Emission Spectroscopy (ICP-OES) and *Inductively Coupled Plasma Mass Spectrometry* (ICP-MS) analyses were carried out using an Agilent 5110 ICP-OES and Agilent 7900 ICP-MS, respectively. For the ICP-OES measurements, the following conditions were applied: Read time: 5 s, RF power: 1.2 kW, stabilization time: 8 s, viewing mode: Axial, viewing height: 8 mm, nebulizer gas flow: 0.65 L/min, plasma flow: 12 L/min, and Aux flow: 1.2 L/min. ICP-MS measurements were performed in no-gas mode. Plasma operation parameters were set as follows: RF power: 1550 W, RF matching: 1.80 V, sample depth: 10 mm, nebulizer gas flow: 0.8 L/min, and dilution gas: 0.4 L/min. Data acquisition parameters included acquisition mode: spectrum, sweeps/replicate: 80, replicates: 3, and integration time/mass: 0.1 sec.

X-ray photoelectron spectroscopy (XPS). All measurements were carried out on a PHI Versa Probe III spectrometer equipped with a monochromatic Al-Kα X-ray source and a hemispherical analyzer (acceptance angle: ±20°). Pass energies of 140 eV and 27 eV, as well as step widths of 0.5 eV and 0.05 eV, were used for survey and detail spectra, respectively. (Excitation energy: 1486.6 eV; Beam energy and spot size: 50 W onto 200 μm; Base pressure: $<8x10^{-10}$ mbar; Pressure during measurements: $<1x10^{-8}$ mbar). Samples were mounted on double-sided polymer tape. Electronic and ionic charge compensation was used for all measurements (automated as provided by PHI). The binding energy (BE) scale and intensity were calibrated using methods described in ISO15472, ISO21270, and ISO24237. Data analysis was performed using CASA XPS and Multipak software packages, employing transmission corrections, Shirley/Tougaard backgrounds [43], and customized Wagner sensitivity factors [44]. The binding energy scale was corrected so SiO_2 is shifted to 103.3 eV BE. Assignment of different components was primarily done using Refs. [45,46].

2.2. Mesoporous SBA-15 silica synthesis

SBA-15 mesoporous silica was synthesized following the procedure outlined by Guillet-Nicolas et al. [31]. Initially, 8.072 g of Pluronic P123 were dissolved in a solution containing concentrated hydrochloric acid (8.025 g, 37 %) and distilled water (146.25 g). The mixture was stirred at 30 °C and 500 rpm overnight until the polymer dissolved completely. Upon complete dissolution of P123, 17.428 g of TEOS were added to the solution, followed by stirring at 30 °C overnight. After 24 h, the solution underwent hydrothermal treatment in Teflon containers within an autoclave for 48 h at 140 °C. The resulting product was subjected to vacuum filtration using Whatman® filter paper (diameter 125 mm) and then dried at room temperature. The resulting white powder was further dried in crucibles at 140 °C for 12 h in a muffle furnace. Once thoroughly dried, the powder was transferred to 250 mL polypropylene (PP) bottles, and ethanol was added to fill one-third of the bottle, along with 1–3 drops of hydrochloric acid (37 %). The suspension was stirred for an additional 45 min at 500 rpm before being vacuum-filtered and dried. Finally, the template was removed through calcination of the powder at 550 °C for 5 h.

2.3. Design of ligand-modified silica

At first, the SBA-15 silica underwent APTES functionalization to introduce $–NH_2$ functionality onto the pore surface. Initially, 0.5 g of SBA-15 were subjected to overnight degassing at 150 °C and then dispersed in 15 mL of anhydrous toluene while stirring at 115 °C under an argon atmosphere. Subsequently, 1 mL of APTES was added, and the reaction mixture was stirred for a minimum of 22 h at 115 °C. The resulting amino-functionalized SBA-15, denoted as $SiO_2\_NH_2$, was retrieved via centrifugation (7500 rpm × 15 min), underwent two toluene washes, two ethanol washes, and was subsequently dried overnight at 85 °C. Then, the amino-functionalized SBA-15 underwent additional modification using pyromellitic dianhydride (Scheme S1). Initially, 0.5 g of pre-dried $SiO_2\_NH_2$, previously dried overnight at 60 °C, were dispersed in 10 mL of anhydrous THF under an argon atmosphere at room temperature. Simultaneously, 0.5 g of PMDA were dissolved in 15 ml of anhydrous THF under argon. Following this, 642 μL of TEA was added to the $SiO_2\_NH_2$ solution, followed by the introduction of the dissolved PMDA solution. The resulting mixture was heated to 50 °C and stirred for a minimum of 22 h under inert conditions. The resulting powder was then collected via centrifugation (7500 rpm × 15 min) and subjected to 3–4 washing cycles using a blend consisting of 80 mL of THF, 20 mL of distilled water, 284 μL of HCl, and a single rinse with technical-grade ethanol. The usage of acid facilitated the generation of carboxyl groups on both the silica surface and within the pores. Finally, the powder was dried overnight at 80 °C. The resulting material is denoted as SiO_2/PMDA.

2.4. Extraction experiments

To generate an adsorption isotherm, 10.1 mg portions of SBA-15 and SiO_2/PMDA powder were exposed to 14.8 mL of Ga or In solution. The solutions were adjusted to pH 3 and maintained at room temperature. The concentration range used to build an isotherm for Ga was 0–200 mg/L, while for In, it was 0–100 mg/L. Initially, the concentration range of 0–100 mg/L for Ga did not produce a plateau on the isotherm curve. Therefore, the concentration range was gradually increased to 150 mg/L and finally to 200 mg/L.

The adsorption capacity at equilibrium was calculated by the given equation (S1):

$$q_e = \frac{C_0 - C_e}{m} \times V \tag{S1}$$

C_o – represents the initial measured concentration of ions (mg/L); C_e represents equilibrium concentration of ions (mg/L); m represents mass of the sorbent (mg); V is the volume of the solution (L).

The isotherms obtained for Ga and In were subjected to fitting with the conventional Langmuir (equation S(2)) and Freundlich (equation S(3)) isotherm models using *non-linear regression*:

$$q_e = q_{max} * \frac{K_L * C_e}{1 + K_L * C_e} \tag{S2}$$

where C_e represents the equilibrium concentration of ions (mg/L); q_m is the maximum adsorption capacity (mg/g); K_L is the Langmuir binding constant (L/g); and q_e is the equilibrium adsorption capacity (mg/g):

$$q_e = K_F * C_e(\frac{1}{n}) \tag{S3}$$

K_F represents the Freundlich empirical constant, expressed in units of (mg/g)/(L/mg)^(1/n), where n is the dimensionless nonlinearity parameter associated with the intensity of adsorption.

For the kinetics test, 10.1 mg of the sorbents were mixed with 14.8 mL of a solution containing Ga (39 mg/L) and In (47 mg/L) at pH 3. The mixtures were then agitated at room temperature for varying durations, ranging from 0 to 1300 min, before concluding the experiment.

The adsorption kinetics of the newly synthesized materials were determined using the pseudo-second-order (S4) kinetic model, which showed a satisfactory fit to the experimental data:

$$\frac{d(q_t)}{d(t)} = k \times (q_e - q_t)^2 \tag{S4}$$

where q_t is the amount of solute adsorbed at time t (mg/g), q_e is the equilibrium adsorption capacity (mg/g), k is the rate constant of pseudo-second-order adsorption (g/mg min).

For the selectivity tests involving Ga and In, 10.1 mg aliquots of SBA-15 sorbent were exposed to 14.8 mL of mixed solutions containing 6, 36, 48, and 60 mg/L of each element at pH=3. Similarly, for the selectivity

tests involving Ga, In, and Zn (a combination of three elements), 10.1 mg aliquots of both sorbents were exposed to 14.8 mL of mixed solutions containing 49 mg/L In, 28 mg/L Ga, and 24 mg/L Zn at pH=3. For the Ga/Al selectivity test, 10.1 mg aliquots of SBA-15 were exposed to 6 mg/L of Ga and Al at pH=3. Lastly, for the selectivity test In/Sn, the 10.1 mg of the modified silica was exposed to 47 mg/L of In and 4.7 mg/L of Sn at pH 2 and at pH 3.

All samples underwent agitation at room temperature for 10,080 min. Subsequently, liquid-phase samples were diluted in 3 % nitric acid, and their contents were analyzed using either an Agilent 5800 ICP-OES or an Agilent 7900 ICP-MS, chosen based on the concentration range being studied and potential interferences of elements in the mixed multi-element solutions. Before ICP-OES analysis, solutions were centrifuged for 30 min at 8000 rpm, followed by dilution, while prior to ICP-MS analysis, samples underwent centrifugation and filtration. All experiments were conducted in triplicate.

For the recyclability test, 10.1 mg of SiO_2/PMDA and SBA-15 powder suspended in an ethanol/water solution was packed into a small Econo-Column® (0.5 × 5 cm, Bio-Rad Laboratories Ges.m.b.H., Austria) applying vacuum underneath the column. Before loading the extraction solution, the powder was conditioned with 5 mL of diluted nitric acid (pH=3). Following this, the Ga extraction solution (260 mg/L for SBA-15, 5 mL) and the In extraction solution (140 mg/L of In for SiO_2/PMDA, 5 mL) were passed through the column using a peristaltic pump (VWR® Peristaltic Pump) with a flow rate of 1.2 mL/min. The captured element was then flushed out from the column with 20 mL of a 0.1 M solution of HNO_3. Subsequently, the column was rinsed and reconditioned with diluted HNO_3 (5 mL, pH=3) before being used for the second extraction. In total, sample underwent 10 cycles of re-use.

The desorption was calculated as shown below:

$$D(\%) = \frac{d}{a} * 100\% \quad \text{(S5)}$$

where d represents the desorption amount (in mg) and a signifies the adsorbed amount of metal (in mg).

When full desorption wasn't accomplished in cycles, the desorption efficiency calculation considered the residual carryover of metal ions from the preceding cycle:

$$D\,(\%) = d_n/(a_n + (a_{(n-1)} - d_{(n-1)})) * 100\% \quad \text{(S6)}$$

In this formula, d_n represents the desorption amount in the current cycle (mg), a_n is the adsorbed amount of metal in the current cycle (mg), and $a_{(n-1)}$ and $d_{(n-1)}$ account for the carryover of metal ions from the previous cycle, where n indicates the cycle number.

3. Results and discussion

3.1. Characterization of developed sorbents

The SBA-15 utilized as a sorbent in this study was synthesized following protocols known for producing high-quality mesoporous silica materials [31]. Subsequently, SBA-15 underwent functionalization with pyromellitic dianhydride using a protocol described above. Low-angle powder X-ray diffraction (PXRD) measurements were conducted to confirm the mesostructured ordering of both SBA-15 and SiO_2/PMDA (Fig. 1a). The X-ray diffractograms of both sorbents showed three distinct diffraction peaks indexed as 100, 110, and 200 reflections, indicative of the two-dimensional (2D) hexagonal mesostructure with a *p6mm* pore symmetry [30]. The diffraction pattern of SiO_2/PMDA closely matched the one of the parent SBA-15, confirming the preservation of the ordered mesoporous structure following surface

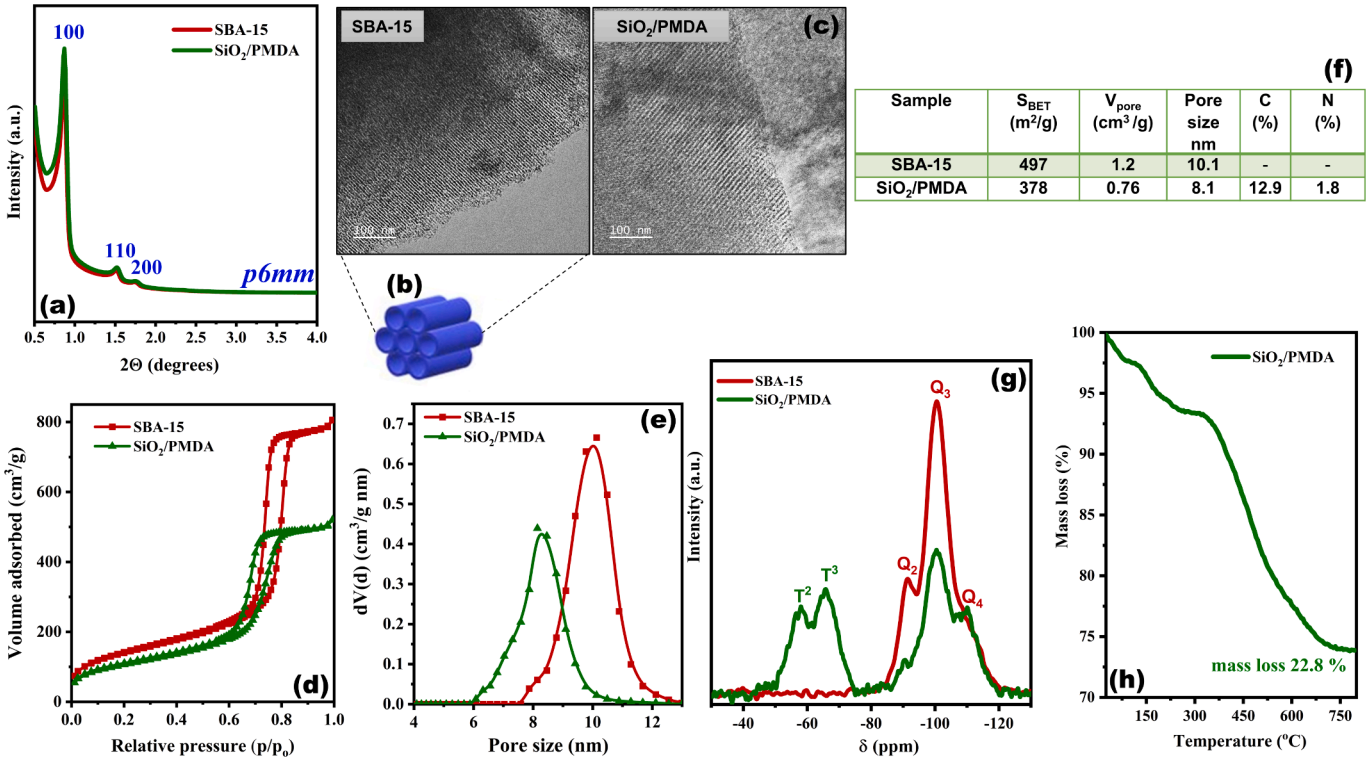

(f)

Sample	S_{BET} (m^2/g)	V_{pore} (cm^3/g)	Pore size nm	C (%)	N (%)
SBA-15	497	1.2	10.1	-	-
SiO_2/PMDA	378	0.76	8.1	12.9	1.8

Fig. 1. (*a*) Low-angle powder XRD patterns of the studied materials. (*b*) Model showing the mesoporous channels in SBA-15. (*c*) TEM images of SBA-15 and SiO_2/PMDA. The scale bar corresponds to 100 nm. (*d*) N_2 adsorption–desorption isotherms at −196 °C for the synthesized materials and (*e*) respective pore size distributions calculated from the equilibrium branch using the NLDFT method (silica with cylindrical pore model). (*f*) Table listing the physicochemical parameters derived from N_2 physisorption measurements at −196 °C and CHN analysis. (*g*) Solid-state ^{29}Si CP/MAS NMR spectra of samples studied (as indicated). (*h*) TGA mass loss profile for the modified silica; the value of mass loss represents the mass loss in the temperature range of 150–800 °C.

modification. TEM images of both sorbents, depicted in Fig. 1c and S1, highlighted the periodic arrangement of channel-like mesopores. Particularly in Figure S1, the hexagonal geometry of these mesopores is clearly discernible for both sorbents, corroborating the observations from the low-angle XRD data.

Both sorbents exhibited typical type IV isotherms in the N_2 physisorption analyses (Fig. 1d). In the relative pressure range (P/P_o) of 0.6–0.8, a steep capillary condensation step with a type H1 adsorption–desorption hysteresis loop was observed. After grafting, the shape of the adsorption–desorption isotherm was well-maintained, but the hysteresis loop shifted to lower values of relative pressure, indicating a decrease in pore size [47]. The NLDFT pore size distributions (Fig. 1e) revealed uniformly sized mesopores for SBA-15 with an average diameter of 10.1 nm (Fig. 1f). After modification, the pore size of SiO_2/PMDA diminished to 8.1 nm (Fig. 1f), revealing the successful incorporation of the grafted ligand within the pores of SBA-15. Furthermore, the specific surface area and pore volume decreased after modification, as illustrated in Fig. 1, Table *f*, further confirming the successful grafting of PMDA onto the silica surface.

The solid-state ^{29}Si CP/MAS NMR spectrum of SBA-15 (Fig. 1g) exhibited signals corresponding to Q^2 and Q^3 sites, indicative of geminal and isolated silanol groups, alongside Q^4 sites integral to the silica network [48–50]. The spectrum for the modified silica displayed additional T^2 and T^3 signals, substantiating the successful chemical modification of the SBA-15 surface. This was further validated by the solid-state ^{13}C CP/MAS NMR spectrum of SiO_2/PMDA (Figure S2), which showed resonance signals at 8, 24, and 48 ppm, attributable to the carbons in the silane propyl chain. Peaks at 132 and 169 ppm correspond to the carbons in the aromatic ring and carbonyl groups, respectively. Furthermore, thermogravimetric analysis (TGA) (Fig. 1h) demonstrated a weight loss of 22.8 wt% for SiO_2/PMDA which is attributed to the thermal decomposition of the grafted organic moieties between 150 and 800 °C, providing conclusive evidence of the PMDA derivative's attachment to the SBA-15 surface. Elemental analysis (Fig. 1f) confirmed the attachment of dianhydride, indicating the presence of carbon and nitrogen in the grafted silica surface.

4. In and Ga adsorption isotherms

After verifying the porosity, structural coherence, and the presence of silanols on the SBA-15 surface and carboxyl groups on the ligand-modified silica, the efficacy of both sorbents for the adsorption of Ga and In from aqueous solutions was investigated. The adsorption capacities of the materials for these ions were determined at equilibrium after immersing the sorbents in aqueous solutions with initial concentrations of the studied elements ranging from 0 to 100 mg/L. To prevent potential precipitation of Ga and In ions at higher pH levels [5,12], a pH of 3 was selected for the experiment. At this pH, positively charged Ga (Ga^{3+}, $GaOH^{2+}$, $Ga(OH)_2^+$, Figure S3) and In (In^{3+}, $InOH^{2+}$, $In(OH)_2^+$) species dominate in the solution [9,13,51], enabling their interaction with non-ionized and deprotonated silanols on SBA-15, as well as ionized and non-ionized COOH groups on ligand-modified silica (Figure S4).

In these experiments, ligand-modified silica exhibited a gradual increase in Ga uptake without reaching a plateau, necessitating an extension of the concentration range to 0–150 mg/L (Fig. 2, *a*). Within this extended concentration range, the ligand-modified silica reached a plateau with an adsorption capacity of approximately ~ 70 mg/g (Fig. 2, *a*). Conversely, bare SBA-15, initially tested under identical conditions, failed to reach saturation at these levels (Figure S5). Upon extending the concentration range to 200 mg/L, adsorption of Ga on SBA-15 reached

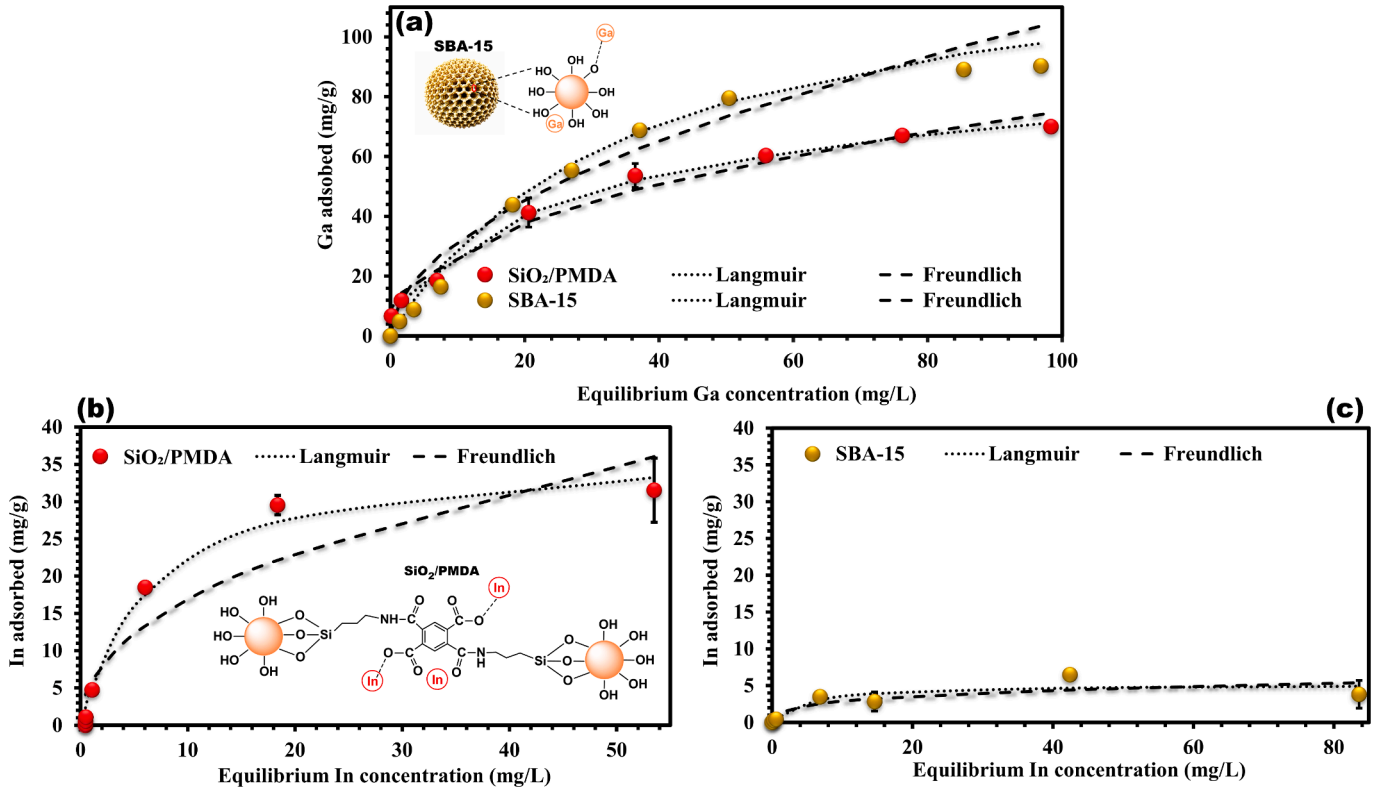

Fig. 2. (*a*) Gallium adsorption isotherms for SBA-15 and SiO_2/PMDA measured in the concentration range of 0–200 mg/L for SBA-15 and 0–150 mg/L for SiO_2/PMDA, analyzed using Langmuir and Freundlich models. The graph includes a schematic illustration of SBA-15 with adsorbed Ga ions. (*b*) Indium adsorption isotherms for SiO_2/PMDA and (*c*) for SBA-15 measured in the concentration range of 0–100 mg/L, analyzed using Langmuir and Freundlich models. The graph includes a schematic illustration of modified silica with adsorbed In ions. All experiments conducted at pH 3 and 25 °C, error bars represent standard deviations from triplicate measurements.

Table 1
Comparison of the gallium adsorption capacity (q_{max}, mg/g) of the studied sorbent with other reported sorbents (the capacities offer a general comparison and should only be regarded as approximate indicators due to the varying conditions (pH, temperature, etc.) applied during the adsorption studies).

Sorbent	Q_{max}, mg/g	Ref.
Amide-functionalized cellulose	~3.3	[12]
Polymeric resin with catechol derivatives	16.4	[16]
Hydrazine amidoxime crosslinked polyacrylonitrile resin	~75.0	[22]
Catechol derivative (Pn)-functionalized cellulose	35.5	[25]
P507@MAC (P507/coconut shell-derived mesoporous activated carbon)	67.0	[27]
Polyacrylic acid/graphene oxide composites:		
PAA@0.3GO-V,	~158.0	[28]
PAA@0.3GO-VIII	~88.0	
GO (graphene oxide)	~70.0	[28]
3D-α-FeOOH (3D hierarchical porous hoya-like α-FeOOH)	52.1	[29]
Modified polymeric resins with catechol derivatives (J1, J2, J3, J4)	16.4, 28.7, 11.1, 16.3	[16]
Amidoximated polyacrylonitrile monolith (C-PAO monolith)	30.8	[53]
$CoFe_2O_4$–Zeolite Material	0.09	[54]
SBA-15	90.0	This work

equilibrium, exhibiting an excellent adsorption capacity of approximately 90 mg/g compared to other sorbents. One of the reported composites, synthesized through oxidation of graphene and its subsequent modification with polyacrylic acid (PAA) ligand, named as PAA@0.3GO-V, as developed by Zhang and coworkers [28], exhibited an adsorption capacity of 158 mg/g at pH=2.8 which is 1.6 times higher than the SBA-15 sorbent (Table 1). However, the synthesis process for this composite is rather complex due to the need for hazardous chemicals to obtain graphene oxide [52]. Furthermore, achieving the desired chemical composition of oxygen-containing groups on graphene oxide may require multiple synthesis attempts before subsequent modifications. In contrast, the synthesis of SBA-15 silica is simpler and involves less toxic chemicals, making it more feasible for large-scale applications. Some sorbents show comparable adsorption capacities, as it is seen from Table 1, while others exhibit significantly lower values. Notably, most of the sorbents presented in the literature are developed through modification of solids, which often incurs additional expenses during the fabrication of new materials.

The high affinity of the SBA-15 surface towards Ga suggests an interaction between the silanol groups of SBA-15 and gallium species as Ga^{3+}, $GaOH^{2+}$, and $Ga(OH)_2^+$. The silica surface is complex, containing isolated, geminal, and vicinal silanols [48]. Previous research has demonstrated that these groups exhibit differences in acidity [55]. Studies by Pfeiffer-Laplaud [56] revealed that convex geminal and certain types of vicinal silanols are sufficiently acidic, with pKa values of 2.9 and 2.1, respectively. In this study, the surface charge of SBA-15 was evaluated by zeta-potential measurements, and the results indeed showed a slightly negative charge for SBA-15 at pH 3 (Figure S4), suggesting the ionization of certain silanol groups. Conversely, concave geminals and isolated groups have been reported to have much higher pKa values of 8.9 and 10.3, respectively [56]. Therefore, silanols with lower pKa values, such as those with pKa values of 2.9 and 2.1, become deprotonated at pH 3 and can interact with positively charged Ga species, possibly forming coordinative bonds. Additionally, positively charged Ga species may interact with non-ionized silanols through electrostatic interactions. This suggests that Ga ions may interact differently with various silanols, forming different types of bonds, thereby contributing to the high adsorption capacity of SBA-15. Furthermore, the larger pores and greater surface area of SBA-15 compared to the ligand-modified sorbent (Fig. 1f) could play a role in enhancing its adsorption performance. These structural characteristics provide additional sites for Ga ion interaction, likely contributing to the observed higher adsorption capacity of bare SBA-15. Strong attraction between hydroxyl groups and Ga ions has been demonstrated in carbon-based sorbents [16,25,57]. While the acidity of carbon phenolic OH groups, typically with a pKa range of 10.8 to 11.8 [58], is generally lower than that of some OH groups on silica surfaces, some silanols on silica still have a pKa of 10.3 [56], similar to that on carbon surfaces allowing a certain comparison.

The adsorption of In ions by unmodified SBA-15 appears to be much less effective (Fig. 2c) than the ligand-modified silica (Fig. 2b). According to Wood et al. [51], in an aqueous environment, these ions form hydrated octahedral complexes. Data from reference [59] suggest that the hydrated octahedral complex of Ga has a radius of approximately 76 pm, while that of In is around 94 pm. Additionally, the higher charge density of Ga^{3+}, due to its smaller size compared to In^{3+}, could result in stronger electrostatic interactions with the functional groups of SBA-15, enhancing its adsorption behavior.

Moreover, as mentioned by Bi and Westerhoff in their study on the adsorption of III/V metals, including In and Ga, on colloidal and fumed SiO_2 as well as other oxide nanoparticles (CeO_2 and Al_2O_3) [11], Ga^{3+} has a higher ionic potential compared to In^{3+} due to its smaller ionic radius and the same + 3 charge. This higher ionic potential could lead to stronger electrostatic attraction to negatively charged sites, such as various silanol groups on the SBA-15 surface, resulting in more effective adsorption of Ga^{3+}. In contrast, In^{3+}, with its larger ionic radius and consequently lower ionic potential, does not interact as strongly with the silanol groups, possibly leading to less effective adsorption on bare SBA-15. The high adsorption efficiency of Ga ions by colloidal and fumed silica was demonstrated by Bi and Westerhoff in their work [11]. Additionally, their study showed a low affinity of colloidal and fumed silica towards In ions, which aligns with our findings. Thus, it can be assumed that the higher ionic potential, smaller octahedrally-coordinated hydrated shell, and higher charge density of Ga could lead to a more favorable interaction with the various silanol groups of the SBA-15 sorbent, resulting in more efficient adsorption of Ga compared to In.

Table 2
Comparison of the indium sorption capacity (q_{max}, mg/g) of the ligand-modified silica with the other sorbents (the capacities offer a general comparison and should only be regarded as approximate indicators due to the varying conditions (pH, temperature, etc.) applied during the adsorption studies).

Sorbent	Q_{max}, mg/g	Ref.
Microagale	16.1	[5]
Pickering emulsion hydrogels (PEHGs)	18.0	[7]
Pyrimidine-based sorbent	214.7	[9]
Methylene crosslinked calix[4]arene tetraacetic acid resin	109.0	[10]
Chitosan-coated bentonite beads	2.9	[23]
Mesoporous activated carbon composite	52.6	[27]
$CoFe_2O_4$-Zeolite Composite	0.09	[54]
Immobilized phosphorylated sawdust bead	0.95	[60]
Poly(vinylphosphonic acid-co-methacrylic acid) microbeads	60.8	[61]
UiO-66	11.8	[62]
Ligand-modified silica (SiO_2/PMDA)	32.0	This work

The In adsorption isotherm constructed for the ligand-modified silica (Fig. 2b) gradually reaches a plateau with an adsorption capacity of ~ 32 mg/g. This value is comparable to those reported for other materials, as shown in Table 2.

One study focusing on In recovery using poly(vinylphosphonic acid-co-methacrylic acid) microbeads [61] (Table 2) reported higher adsorption capacities compared to the ligand-modified silica presented in this work, achieving 0.53 mmol/g, equivalent to 60.8 mg/g [61]. Nevertheless, the adsorption of In with these microbeads was studied at pH 8, markedly different from the pH 3 employed in our study. Similarly, pyrimidine-based sorbent [9] exhibited high adsorption capacity of 214.7 mg/g, as it can be seen from Table 2, but the adsorption occurred at pH 4. Notably, as pH decreases to 3, as used in this work, the concentration of H^+ increases, intensifying competition with In ions and resulting in reduced adsorption capacity [28]. Additionally, the surface charge of the ligand-modified silica becomes less negative at lower pH levels (Figure S4) due to a decreased amount of deprotonated COOH groups and an increased amount of protonated COOH groups. This leads to a reduced adsorption capacity of the ligand-modified silica sorbent at lower pH.

The good affinity of the ligand-modified silica surface towards In suggests interaction with the carboxyl groups of the sorbent. At pH 3, some COOH groups of the pyromellitic anhydride derivative on the silica surface become deprotonated, acquiring a strong negative charge (Figure S4) as it is mentioned above. The ionized carboxylates can form coordinative covalent bonds with positively charged In species (mainly In^{3+}, and to a lesser extent $InOH^{2+}$ and $In(OH)_2^+$ due to their lower concentrations in the solution). Additionally, non-ionized carboxyl groups with partial negative charge may engage in electrostatic interactions with In ions, further enhancing affinity. This aligns with prior research [5,61,62], where carboxyl-containing sorbents like microalgae, poly(vinylphosphonic acid-co-methacrylic acid) microbeads, and UiO-66 also show good affinity towards In ions.

The adsorption isotherms of Ga and In ions for both sorbents were modeled using Langmuir and Freundlich isotherms. The Langmuir model showed a better fit to the experimental data, as evidenced by the higher R^2 values indicated in Table S1. This agreement implies that the adsorption sites on the sorbent surfaces are finite, homogeneous, and facilitate monolayer sorption processes [47]. Given SBA-15's excellent adsorption capacity for Ga ions and the ligand-modified silica's capacity for In ions, subsequent tests focused on the adsorption studies of SBA-15 with Ga and ligand-modified silica with In.

5. Kinetics studies

As illustrated in Fig. 3a, the adsorption kinetics of Ga ions on SBA-15 exhibit a gradual increase before reaching equilibrium within 240 min. This timeframe is rapid compared to other studies, such as one utilizing modified chitosan-silica adsorbent which required 8 h [63], and cellulose adsorbent which required 24 h [25] to reach equilibrium. In contrast, there is a report on propionylamino -functionalized cellulose achieving equilibrium in only 3 min [12]. However, modifying cellulose with propionylamino functionalities requires the use of additional chemicals that might incur extra expenses and is time-consuming.

As it is shown in Fig. 3b, the rapid uptake of In ions by ligand-modified silica is observed within the first 22 min, with the sorbent reaching full saturation capacity (~35 mg/g) within 43 min which is well within the range of other published experimental In sorbents [5]. Fast kinetics are important for process scale-up, as with rapid adsorption, smaller reactor volumes are required, ensuring efficiency and cost-effectiveness [5].

Both kinetic analyses for SBA-15 and SiO_2/PMDA with studied Ga and In ions, respectively, closely match the pseudo-second-order kinetic model, as indicated by the high R^2 values of 0.99 (Table S2) for SiO_2/PMDA and 0.99 for SBA-15. This suggests that the adsorption process might be predominantly driven by chemisorption, where the rate decreases as the number of available adsorption sites diminishes [22,64]. However, studies by Simonin [65] and Hubbe et al. [66] highlight that a good fit to the pseudo-second-order model alone does not conclusively validate chemisorption as the primary mechanism. These studies emphasize the need to consider additional factors and experimental conditions, such as diffusion processes and the variability of sorbate concentration during the adsorption, which could also significantly influence the overall adsorption kinetics. Therefore, further investigation is needed to fully understand the adsorption mechanisms involved.

6. Selectivity studies

6.1. Recovery of Ga from solution reflecting the Ga/In/Zn concentration in semiconductor targets

Given the extensive use of Ga, In, and Zn in the semiconductor industry [38–40], the sorbents were assessed for their capacity to separate one of these elements from another. The elemental ratios were chosen based on reported measured values of each element found in indium, gallium, and zinc oxide semiconductor target materials [67]. From Fig. 4a, it is apparent that SBA-15 exhibits a preference for adsorbing Ga ions over In ions, with an adsorption capacity of approximately ~ 20 mg/g for Ga and only ~ 8 mg/g for In. Indium was present at a much higher concentration (49 mg/L) compared to Ga ions (28 mg/L) in this solution, further confirming the excellent affinity of SBA-15 specifically for Ga ions. The sorbent demonstrated no adsorption of Zn ions, effectively separating Ga from Zn, thereby improving upon previous reports [68]. In contrast, ligand-modified silica exhibits a preference for In over

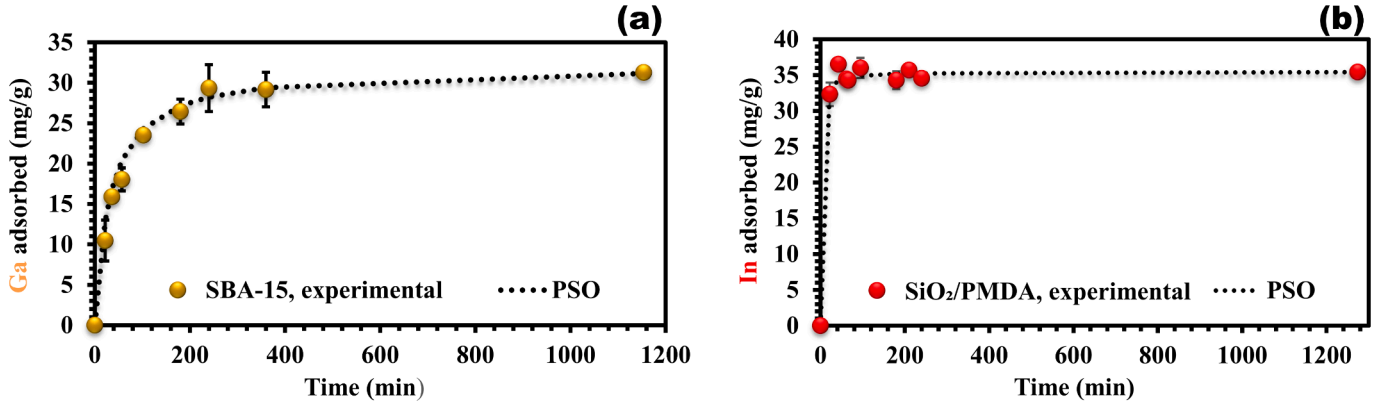

Fig. 3. Impact of contact time on Ga adsorption by SBA-15 (*a*, depicted by gold-colored points) and In adsorption by modified silica (*b*, depicted by red-colored points) at initial concentrations of Ga (39 mg/L) and In (47 mg/L), analyzed with the pseudo-second-order (PSO) model and depicted as dotted lines. All experiments conducted at pH 3 and 25 °C, error bars represent standard deviations from triplicate measurements.

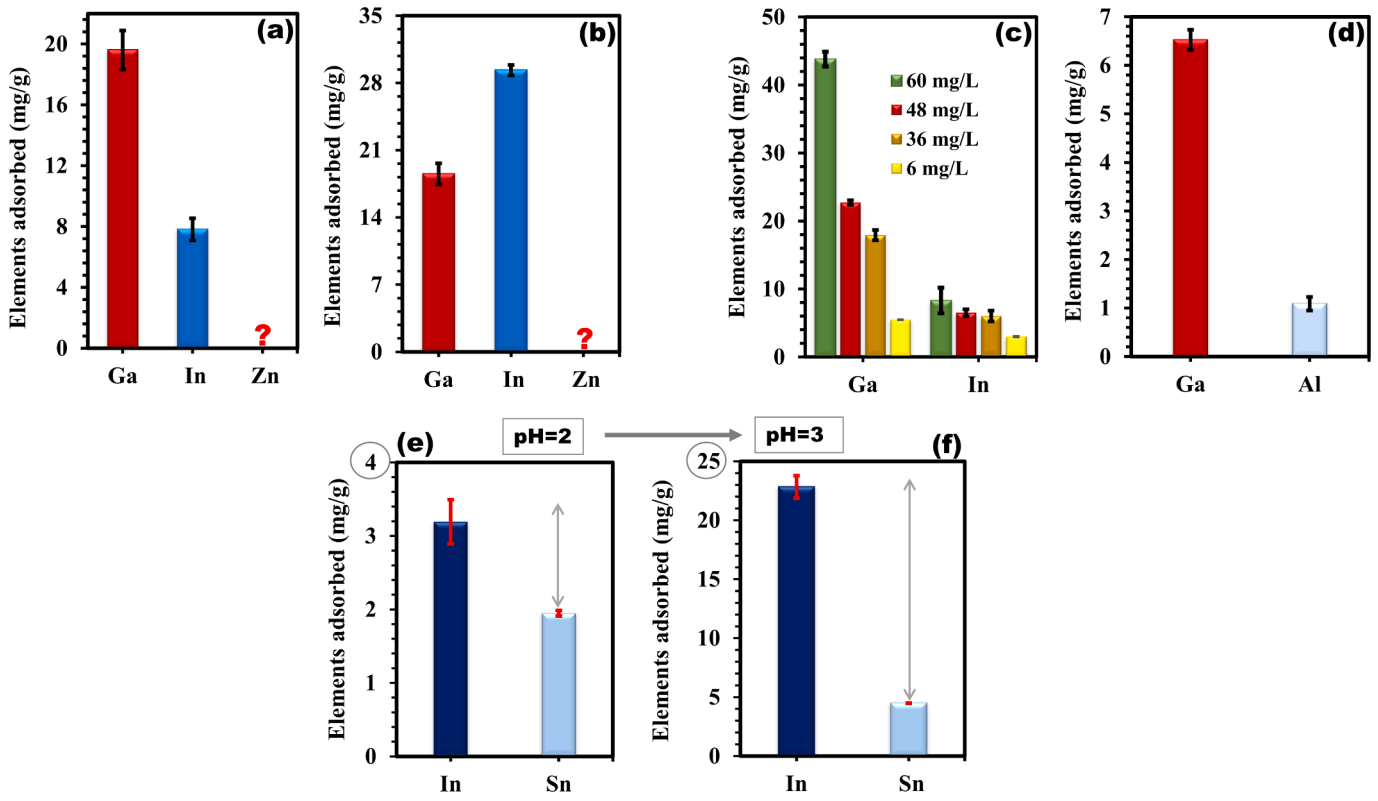

Fig. 4. (a) The adsorption of Ga (28 mg/L), In (49 mg/L), and Zn (24 mg/L) solution by SBA-15, and by (b) SiO_2/PMDA, with the concentrations reflecting the actual concentration ratio between these elements in In, Ga, and ZnO semiconductor target materials [67]. The question mark signifies no affinity of the sorbents towards Zn ions. (c) Adsorption of Ga and In ions by SBA-15, with the concentration of elements indicated on the graph and (d) adsorption of Ga and Al ions by SBA-15 with each element at a concentration of 6 mg/L. The tests were conducted at pH 3 and a temperature of 25 °C. (e, f) Adsorption of In and Sn by SiO_2/PMDA at pH 2 and pH 3 (as indicated on the graphs) and at a temperature of 25 °C. The concentration of In in the solution was 47 mg/L, while the concentration of Sn was 4.7 mg/L, reflecting the actual concentration ratio between these elements in ITO [70]. Error bars in all graphs represent the standard deviation of triplicate measurements.

Ga (Fig. 4b), demonstrating a difference in adsorption capacity of 10 mg/g between these two elements. The sorbent also reveals excellent separation of In from Zn, as depicted in Fig. 4b. The absence of Zn adsorption in the presence of Ga and In suggests that these ions interfere with the adsorption of Zn. The lack of adsorption of Zn by SBA-15 and ligand-modified silica may be due to the higher affinity of carboxyl and silanol groups towards In and Ga species. This difference in affinity can be attributed to the distinct charges and speciation of In and Ga ions compared to Zn ions. In a solution at pH 3, Ga and In predominantly exist as Ga^{3+}, $GaOH^{2+}$, $Ga(OH)_2^+$ (Figure S3), and In^{3+}, $InOH^{2+}$, $In(OH)_2^+$ ions, respectively [51]. In contrast, Zn primarily exists as Zn^{2+} (Figure S6). Furthermore, a previous study has reported that Zn adsorption increases with increasing pH to 6.0 [69].

6.2. Recovery of Ga from Ga/In binary solutions

Given the wide utilization of Ga and In in solar cells [8,22], the effective separation of Ga from In is of high importance. In this study, four binary solutions containing Ga and In were prepared, and SBA-15 was evaluated for its preferential affinity towards Ga in the presence of In ions, ranging from 6 mg/L to 60 mg/L concentrations for each element (Fig. 4c). With increasing concentrations of both elements, the separation efficiency notably improved. At lower concentrations of Ga and In, i.e., 6 mg/L, Ga exhibited 1.8 times greater adsorption than In. This trend continued as the concentrations increased. At 36 mg/L, Ga showed 3 times more adsorption than In, while at 48 mg/L, the separation efficiency of SBA-15 revealed a ratio of 3.5, indicating Ga adsorption was 3.5 times higher than In. The most notable separation between Ga and In ions occurred at a concentration of 60 mg/L for both elements, as depicted by the green bar in Fig. 4c. Here, SBA-15 exhibited an adsorption capacity of 44 mg/g for Ga and only 8 mg/g for In, highlighting its superior affinity for Ga over In by approximately 5.3 times. This remarkable separation performance is particularly notable in light of the scarcity of previous studies utilizing SPE sorbents specifically for the challenge of separating Ga from In. Furthermore, this selectivity is achieved using bare silica, SBA-15, a greener alternative to previously reported materials with complex functionalized surfaces [12,16,24,53,54].

6.3. Recovery of Ga from Ga/Al binary solution

In addition to In, Al is one of the main competitive elements when Ga is recovered from waste streams derived from the aluminum production industry [42]. SBA-15 shows excellent separation efficiency adsorbing Ga 6 times higher than Al showing an adsorption capacity for Ga ~ 6.5 mg/g and ~ 1.1 mg/g for Al (Fig. 4d). The difference in the adsorption of Al and Ga on the SBA-15 surface may be attributed to the difference in the hydrated shell radius of Al and Ga, which is larger for Ga [59]. Both ions form octahedral complexes in an aqueous environment [51,71]. However, Ga^{3+}, with its larger hydrated ionic radius, appears to be more suitable for binding with the silanol groups on the SBA-15 surface. This likely leads to the formation of a specific stable complex with Ga, which is not as easily formed with Al due to its smaller size and different complexation behavior. Additionally, other species of Ga, such as $GaOH^{2+}$ and $Ga(OH)_2^+$, can interact with both non-ionized and ionized silanol groups of SBA-15, contributing to overall adsorption. In contrast, at pH 3, Al exists predominantly as Al^{3+} (Figure S7), differing from the species present for Ga at this pH.

6.4. Recovery of In from a binary solution reflecting the concentrations of In and Sn in ITO elements

Given the extensive use of In in indium tin oxide production, the selectivity of ligand-modified silica towards In in the presence of Sn was examined. As illustrated in Fig. 4e,f at pH 2, the adsorption of In ions was 1.6 times higher compared to Sn ions (Sn^{2+} and $SnOH^{+}$, Figure S8). With a rise in pH to 3 (Fig. 4f), the separation efficiency is further enhanced, yielding adsorption capacities of approximately 23 mg/g for In and ~ 4.5 mg/g for Sn. Clearly, the adsorption of In at pH 3 shows a significant increase compared to pH 2, while the adsorption of Sn shows only a slight increase from pH 2 to pH 3. The reduced adsorption performance at pH 2, compared to pH 3, can be ascribed to the surface of the material acquiring a positive charge at lower pH levels (Figure S4). This positive charge likely repels positively charged metal ions through electrostatic interactions. At higher pH, the ligand-modified silica surface loses its positive charge and instead acquires a strong negative charge (Figure S4), which can attract In and Sn species from the solution. This also suggests that In ions adsorption onto ligand-modified silica primarily involves interaction with carboxyl groups. Alternatively, if carbonyl groups were also involved in chelating In ions during adsorption, their effectiveness is unlikely to be affected by pH variations, resulting in the same adsorption capacities of ligand-modified silica for In at both pH. It is worth mentioning that, given the higher concentration of In in the ITO solution compared to Sn, greater adsorption of In over Sn can be expected. However, as illustrated earlier in Fig. 4a, in a solution where In was present at a concentration of 49 mg/L and Ga at a much lower concentration of 28 mg/L, the sorbent still demonstrated selective adsorption of Ga despite the higher concentration of In. This trend aligns with previous reports [5]. The study showed selective extraction of In in binary solutions such as In/Zn, In/Al, and In/Sn. Despite the competing ions being present at concentrations ten times higher, the sorbent exhibited selective adsorption of In over the competing elements [5]. This result suggests that the sorbent's selectivity remains consistent regardless of the concentration of the target element or competing elements. In other words, the sorbent's selectivity is determined by the interplay between the chemical properties of the ions and the functional groups involved in their interaction, not only the concentration of the elements.

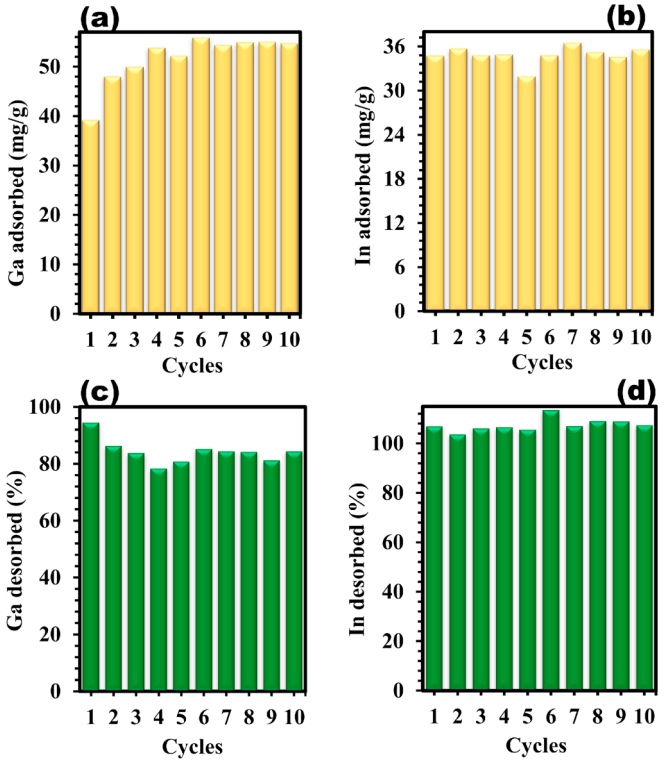

Fig. 5. Reusability performance of SBA-15 (*a*: adsorption, *c*: desorption) with Ga ions (260 mg/L) and ligand-modified silica (*b*: adsorption, *d*: desorption) with In ions (140 mg/L) over 10 cycles in a dynamic system. Desorption was carried out using 0.1 M HNO_3. The conditioning solution used before each new cycle was 0.001 M HNO_3. All tests were conducted at pH 3 and at room temperature.

7. Reusability studies

To further demonstrate the potential industrial applicability of both materials, their reusability was investigated (Fig. 5a,b). During the re-use test of Ga extraction by SBA-15, the adsorption capacity was slightly lower across the first three cycles but stabilized from cycles 4 to 10 (Fig. 5a). This behavior could suggest that the sorbent reaches a certain level of conditioning or equilibrium after several cycles, leading to stabilized adsorption capacity from cycles 4 to 10. While full desorption was not achieved in each cycle for SBA-15 (Fig. 5c), it did not affect the adsorption abilities of the sorbent, which exhibited good adsorption through all cycles (Fig. 5a). Similarly, ligand-modified silica (SiO_2/PMDA) exhibited a good re-use profile (Fig. 5b), maintaining a stable adsorption capacity for In ions across all cycles, with full desorption achieved in each cycle (Fig. 5d). The use of 0.1 M HNO_3 as a desorption agent further confirmed the stability of both sorbents. The consistent performance of the sorbents, despite being subjected to an acidic environment ten times during desorption tests, demonstrated excellent acid stability of the sorbents.

8. XPS studies on In and Ga interaction with functional groups of the sorbents

The O1s spectrum (Figure S9a) for SBA-15 shows a peak at 532.2 eV, while the O1s spectrum for SBA-15 loaded with Ga species shows a peak at 532.8 eV with a broadening effect. This broadening suggests the presence of multiple oxygen environments, indicating potential interactions between the oxygen atoms and the gallium species, likely involving the interaction of Ga with the oxygen atoms of the silanol groups (Si-OH) on the surface. The Si2p XPS spectra (Figure S9b) for both bare SBA-15 and SBA-15 loaded with Ga species demonstrate that the silicon environment remains unchanged upon Ga loading. The binding energy peak at 103.4 eV is consistent across both samples, with no significant broadening or shifts. This suggests that Ga interactions occur primarily at the surface silanol groups, which do not disturb most of the silicon atoms in the silica framework. This is expected, as Si atoms do not primarily interact with Ga ions; instead, the oxygen atoms do, which does not significantly influence the electronic environment of silicon.

The analysis of the Ga 3d binding energies (Figure S9c, bottom) and Ga LMM Auger-Meitner kinetic energies (Figure S9c, top) indicates that the gallium species present in the sample are not in the form of metallic Ga or common Ga oxides/hydroxides. This is supported by a comparison with reference data from the NIST XPS database [45], which showed different binding energies and kinetic energy values for these states. Therefore, the gallium in the sample likely exists in a different chemical form, potentially defined by its interaction with the surface silanol groups of the SBA-15 material, as supported by the O1s spectrum.

The O1s XPS spectrum (Figure S10, *a*, bottom) for SiO_2/PMDA exhibits a peak at a binding energy of 532.6 eV. For the SiO_2/PMDA sample loaded with In species (Figure S10, *a*, top), the O1s XPS spectrum shows a peak at 532.6 eV with noticeable broadening compared to the pure SiO_2/PMDA sample. This broadening effect indicates potential interactions between the oxygen atoms and the indium species. Additionally, no metal oxide peaks are found in the O1s spectrum of In, as no peak is observed around 529–530 eV, suggesting that In is not in the oxide form on the sorbent surface. The C1s XPS spectrum (Figure S10, *b*,

bottom) of the SiO_2/PMDA sample shows binding energies at 284.9 eV (C-C), 286.2 eV (C-O-C/COOH), and 288.4 eV (O-C=O), confirming the presence of the grafting ligand on the SBA-15 surface. This is consistent with the C^{13} SS NMR spectrum (Figure S2). Upon loading with In species, the C1s spectrum shows binding energies at 284.9 eV (C-C), 286.2 eV (C-O-C/COOH), and 288.6 eV (O-C=O), with a broadening effect suggesting potential interactions between the carbon–oxygen atoms and the indium species. The Si2p XPS spectra (Figure S10c) for both SiO_2/PMDA and SiO_2/PMDA+In show that the silicon environment remains unchanged upon In loading. The binding energy peak at 103.2 eV for SiO_2/PMDA shows no broadening, compared to the peak at 103.3 eV for SiO_2/PMDA+In. This could indicate that indium interactions occur primarily at the surface COOH groups and do not disturb silicon atoms in the silica framework, as shown for SBA-15 and Ga above.

Binding/kinetic energies taken from In3d and In LMM Auger-Meitner spectra (Figure S11a and b) are combined and shown in the Wagner plot in Figure S11c. The most probable bonding environment of In is identified as In-O interaction, as indicated by the orange circle on the Wagner plot (data taken from NIST X-ray photoelectron spectroscopy database [45]). This result suggests that the primary interaction of In is with oxygen. However, it is currently indeterminate whether this oxygen originates from the OH group of COOH or from carbonyl oxygen, requiring further investigation.

9. Conclusions

In this study, we demonstrated the efficacy of bare SBA-15 and ligand-modified silica as efficient sorbents for recovering Ga and In from diverse multi-element solutions including their main competing elements.

Bare SBA-15 silica displayed exceptional adsorption capacity for Ga ions, achieving ~ 90 mg/g at pH 3, surpassing previous reports on Ga adsorption. In contrast, ligand-modified silica proved effective in extracting In ions, with a capacity of ~ 32 mg/g. The sorbents exhibit efficient adsorption kinetics, with Ga adsorption reaching equilibrium in 240 min for SBA-15 and In achieving equilibrium in only 43 min for the ligand-modified silica, highlighting their rapid adsorption capabilities compared to prior research. Moreover, SBA-15 showed remarkable selectivity for Ga in a solution containing Ga, In, and Zn, even with a higher concentration of In. This selectivity, along with the sorbent's lack of affinity for Zn, can significantly advance Ga recovery from semiconductor targets composed of In/Ga/Zn. Additionally, the sorbent efficiently separates Ga from Al, crucial for recovering Ga from aluminum production waste streams. In binary solutions with Ga and In ions ranging from 6 to 60 mg/L, SBA-15 demonstrated excellent separation, especially at higher concentrations.

The ligand-modified silica, on the other hand, demonstrated effective selective adsorption of In in solutions containing Ga, In, and Zn, showing better affinity towards In compared to Ga and exhibiting excellent separation between In and Zn. The ligand-modified sorbent also exhibited effective In adsorption in a binary solution containing In and Sn ions, thereby advancing the recovery of In from ITO films. This wide-ranging effectiveness, coupled with sorbents good reusability, highlights the potential of these materials for diverse industrial applications.

CRediT authorship contribution statement

Iryna Protsak: Writing – review & editing, Writing – original draft, Visualization, Validation, Resources, Project administration, Methodology, Investigation, Funding acquisition, Formal analysis, Data curation, Conceptualization. **Martin Stockhausen:** Writing – review & editing, Resources, Formal analysis, Validation, Funding acquisition. **Aaron Brewer:** Writing – review & editing, Validation, Funding acquisition, Formal analysis. **Martin Owton:** Writing – review & editing, Formal analysis, Methodology, Validation. **Thilo Hofmann:** Writing – review & editing, Validation, Formal analysis, Resources, Funding acquisition. **Freddy Kleitz:** Writing – review & editing, Validation, Formal analysis, Resources, Funding acquisition.

Declaration of competing interest

The authors declare that they have no known competing financial interests or personal relationships that could have appeared to influence the work reported in this paper.

Data availability

The datasets supporting the results presented in the paper can be found under the following link (Open Science Framework): DOI 10.17605/OSF.IO/JVHXE.

Acknowledgements

This research was funded in whole by Austrian Science Fund (FWF) [DOI 10.55776/ESP30, available via https://www.fwf.ac.at/en/discover/ research-radar]. Dr. Aaron Brewer acknowledges the support of the FWF Lise Meitner Grant (M 2750-N). For ICP-OES and ICP-MS analyses at the Bioanalytics and Environmental Mass Spectrometry Facility, Thilo Hofmann and Martin Stockhausen acknowledge funding from the Austrian Science Fund, Cluster of Excellence CoE7, Grant-DOI 10.55776/COE7. The authors thank Prof. Hanspeter Kählig (Faculty of Chemistry, University of Vienna) for support with SS NMR measurements. The authors thank Prof. Annette Foelske and Dr. Markus Sauer (Analytical Instrumentation Center at Vienna University of Technology) for their support with XPS measurements, which were carried out using equipment acquired with the support of the Österreichische Forschungsförderungsgesellschaft (FFG) under the project 'ELSA' (project n° 884672).

Appendix A. Supplementary data

Supplementary data to this article can be found online at https://doi.org/10.1016/j.cej.2024.154468.

References

[1] European Commission, Study on the Critical Raw Materials for the EU 2023 – Final Report.
[2] European Commission, Study on the EU's List of Critical Raw Materials 2020 – Final Report.
[3] European Commission, Communication from the Commission to the European Parliament, The Council, the European Economic and Social Committee, and the Committee of the Regions on the 2017 list of Critical Raw Materials for the EU.
[4] European Commission, Report on Critical Raw Materials for the EU 2014 – Final Report.
[5] N.R. Nicomel, L. Otero-Gonzalez, L. Arashiro, M. Garfí, I. Ferrer, P. Van Der Voort, K. Verbeken, Microalgae: a sustainable adsorbent with high potential for upconcentration of indium (III) from liquid process and waste streams, Green Chem. 22 (2020) 1985–1995, https://doi.org/10.1039/C9GC03073E.
[6] A. Brewer, J. Florek, F. Kleitz, A perspective on developing solid-phase extraction technologies for industrial-scale critical materials recovery, Green Chem. 24 (2022) 2752–2765, https://doi.org/10.1039/D2GC00347C.
[7] C. Dong, J. Gao, Y. Zhao, T. Tian Ma, Y. He, Preparation of a novel sorbent based on pickering emulsions polymerization method for encapsulating extractants and the adsorption of indium in an aqueous solution, Macromol. Chem. Phys. 224 (2023) 2300002, https://doi.org/10.1002/macp.202300002.
[8] J. Ramanujam, U.P. Singh, Copper indium gallium selenide based solar cells – a review, Energy Environ. Sci. 10 (2017) 1306–1319, https://doi.org/10.1039/C7EE00826K.
[9] M.F. Hamza, A.A.M.A. El-Hamid, E. Guibal, A.A.H. Abdel-Rahman, R.E. Araby, Synthesis of a new pyrimidine-based sorbent for indium (III) removal from aqueous solutions – application to ore leachate, Sep. Purif. Technol. 314 (2023) 123514, https://doi.org/10.1016/j.seppur.2023.123514.
[10] B.B. Adhikari, M. Gurung, H. Kawakita, K. Ohto, Solid-phase extraction, preconcentration, and separation of indium with methylene crosslinked calix[4]- and calix[6]arene carboxylic acid resins, Chem. Eng. Sci. 78 (2012) 144–154, https://doi.org/10.1016/j.ces.2012.05.023.

[11] X. Bi, P. Westerhoff, Adsorption of III/V Ions (In(III), Ga(III), and As(V)) onto SiO_2, CeO_2, and Al_2O_3 nanoparticles used in the semiconductor industry, Environ. Sci. Nano 3 (2016) 1014–1026, https://doi.org/10.1039/C6EN00184J.

[12] W. Guo, J. Zhang, F. Yang, F. Tan, Z. Zhao, Highly efficient and selective recovery of gallium achieved on an amide-functionalized cellulose, Sep. Purif. Technol. 237 (2020) 116355, https://doi.org/10.1016/j.seppur.2019.116355.

[13] H.V. Thanh Luong, J.C. Liu, Flotation separation of gallium from aqueous solution – effects of chemical speciation and solubility, Sep. Purif. Technol. 13 (2014) 115–119, https://doi.org/10.1016/j.seppur.2014.04.054.

[14] A.N. Løvik, E. Restrepo, D.B. Müller, The global anthropogenic gallium system: determinants of demand, supply, and efficiency improvements, Environ. Sci. Technol. 49 (2015) 5704–5712, https://doi.org/10.1021/acs.est.5b00320.

[15] H.-M. Liu, C.-C. Wu, Y.-H. Lin, C.-K. Chiang, Recovery of indium from etching wastewater using supercritical carbon dioxide extraction, J. Hazard. Mater. 172 (2009) 744–748, https://doi.org/10.1016/j.jhazmat.2009.07.098.

[16] P. Raj, M. Patel, A.K. Karamalidis, Chemically modified polymeric resins with catechol derivatives for adsorption, separation, and recovery of gallium from acidic solutions, J. Environ. Chem. Eng. 11 (2023) 110790, https://doi.org/10.1016/j.jece.2023.110790.

[17] X. Wu, S. Wu, W. Qin, X. Ma, Y. Niu, S. Lai, C. Yang, F. Jiao, L. Ren, Reductive leaching of gallium from zinc residue, Hydrometall. 113–114 (2012) 195–199, https://doi.org/10.1016/j.hydromet.2011.11.016.

[18] S. Saikia, A. Sinharoy, P.N.L. Lens, Adsorptive removal of gallium from aqueous solution onto biogenic elemental tellurium nanoparticles, Sep. Purif. Technol. 286 (2022) 120462, https://doi.org/10.1016/j.seppur.2022.120462.

[19] Y. Yuan, Y. Yang, K.R. Meihaus, S. Zhang, X. Ge, W. Zhang, R. Faller, J.R. Long, G. Zhu, Selective scandium ion capture through coordination templating in a covalent organic framework, Nat. Chem. 15 (2023) 1599–1606, https://doi.org/10.1038/s41557-023-01273-3.

[20] A. Brewer, C. Reicher, O. Manatschal, H. Bai, K. Nakanishi, F. Kleitz, Powdered hierarchically porous silica monoliths for the selective extraction of scandium, ACS Sustainable Chem. Eng. 11 (2023) 15432–15439, https://doi.org/10.1021/acssuschemeng.3c04672.

[21] Z. Wang, A.T. Brown, K. Tan, Y.J. Chabal, K.J. Balkus Jr., Selective extraction of thorium from rare earth elements using wrinkled mesoporous carbon, J. Am. Chem. Soc. 140 (2018) 14735–14739, https://doi.org/10.1021/jacs.8b07610.

[22] Z. Qin, S. Wang, L. Fan, C.-A. Zhou, C. Wang, L. Song, K. Ma, H. Yue, A hydrazine amidoxime crosslinked polyacrylonitrile resin for efficient extraction of gallium from vanadium-containing waste solution, Chem. Eng. Sci. 282 (2023) 119240, https://doi.org/10.1016/j.ces.2023.119240.

[23] M.J.C. Calagui, D.B. Senoro, C.-C. Kan, J.W.L. Salvacion, C.M. Futalan, M.-W. Wan, Adsorption of indium (III) ions from aqueous solution using chitosan-coated bentonite beads, J. Hazard. Mater. 277 (2014) 120–126, https://doi.org/10.1016/j.jhazmat.2014.04.043.

[24] S. Chegrouche, A. Bensmaili, Removal of Ga (III) from aqueous solution by adsorption on activated bentonite using a factorial design, Water Res. 36 (2022) 2898–2904, https://doi.org/10.1016/S0043-1354(01)00498-5.

[25] P. Raj, M. Patel, A.K. Karamalidis, Functionalization of cellulose adsorbents with catechol derivatives for the effective separation and recovery of gallium from acidic solutions, Sep. Purif. Technol. 323 (2023) 124396, https://doi.org/10.1016/j.seppur.2023.124396.

[26] F.J. Alguacil, F.A. Lopez, O. Rodriguez, S. Martinez-Ramirez, I. Garcia-Diaz, Sorption of indium (III) onto carbon nanotubes, Ecotoxicol. Environ. Saf. 130 (2016) 81–86, https://doi.org/10.1016/j.ecoenv.2016.04.008.

[27] W. Wang, X. Xu, D. Lai, Q. Xu, J. Li, Y. Wang, Selective isolation of gallium and indium from waste photovoltaic modules facilitated by extractant-mesoporous activated carbon composites, Sep. Purif. Technol. 330 (2024) 125510, https://doi.org/10.1016/j.seppur.2023.125510.

[28] Y. Zhang, X. Liu, Y. Wang, Z. Lou, W. Shan, Y. Xiong, Polyacrylic acid-functionalized graphene oxide for high-performance adsorption of gallium from aqueous solution, J. Colloid Interface Sci. 556 (2019) 102–110, https://doi.org/10.1016/j.jcis.2019.08.032.

[29] X. Wu, M. Yuan, X. Guo, L. Zhang, Fast coadsorption and selective separation of gallium(III) and germanium(IV) from aqueous solutions by 3D hierarchical porous hoya-like α-FeOOH, ACS Sustainable Chem. Eng. 7 (2019) 15939–15947, https://doi.org/10.1021/acssuschemeng.9b02199.

[30] D. Zhao, J. Feng, Q. Huo, N. Melosh, G.H. Fredrickson, B.F. Chmelka, Triblock copolymer syntheses of mesoporous silica with periodic 50 to 300 angstrom pores, Science 279 (1998) 548–552, https://doi.org/10.1126/science.279.5350.548.

[31] R. Guillet-Nicolas, F. Bérubé, M. Thommes, M.T. Janicke, F. Kleitz, Selectively tuned pore condensation and hysteresis behavior in mesoporous SBA-15 silica: correlating material synthesis to advanced gas adsorption analysis, J. Phys. Chem. C 121 (2017) 24505–24526, https://doi.org/10.1021/acs.jpcc.7b06745.

[32] R. Yildiz, Y. Lorgouilloux, J. Dhainaut, C. Ciotonea, J.-P. Dacquin, S. Royer, C. Courtois, Assembly of SBA-15 into hierarchical porous monoliths replicating polymeric scaffolds, Micropor. Mesopor. Mat. 337 (2022) 111908, https://doi.org/10.1016/j.micromeso.2022.111908.

[33] D.-Y. An, W.-R. Pu, Y. Wang, X. Zhang, Y.-P. Huang, Z.-S. Liu, Improving sorption performance of a molecularly imprinted monolithic column by doping mesoporous molecular sieve SBA-15, Microchim Acta 189 (2022) 85, https://doi.org/10.1007/s00604-022-05192-x.

[34] N. Huang, X. Chen, R. Krishna, D. Jiang, Two-dimensional covalent organic frameworks for carbon dioxide capture through channel-wall functionalization, Angew. Chem. Int. Ed. 127 (2015) 3029–3033, https://doi.org/10.1002/anie.201411262.

[35] A. Sthoer, E.M. Adams, S. Sengupta, R.W. Corkery, H.C. Allen, E.C. Tyrode, La^{3+} and Y^{3+} interactions with the carboxylic acid moiety at the liquid/vapor interface: identification of binding complexes, charge reversal, and detection limits, J. Colloid Interface Sci. 608 (2022) 2169–2180, https://doi.org/10.1016/j.jcis.2021.10.052.

[36] D. Saha, V. Bhasin, S. Khalid, N. Smeriglio, S. Cuka, D. Bhattacharyya, J. Rodgers, P. Panja, M. Deo, T. Apple, Adsorption of rare earth elements in carboxylated mesoporous carbon, Sep. Purif. Technol. 314 (2023) 123583, https://doi.org/10.1016/j.seppur.2023.123583.

[37] I. Protsak, M. Stockhausen, A. Brewer, M. Owton, T. Hofmann, F. Kleitz, Advancing selective extraction: a novel approach for scandium, thorium, and uranium ion capture, Small Sci. (2024) 2400171, https://doi.org/10.1002/smsc.202400171.

[38] Y. Xu, B. Deng, S. Kuang, W. Liao, Selective extraction and separation of gallium (III) from indium(III) in chloride medium using Di(2-ethylhexyl) (N, N′-di(2-ethylhexyl) amino methyl) phosphonate and stripping with water, Hydrometall. 217 (2023) 106035, https://doi.org/10.1016/j.hydromet.2023.106035.

[39] D.-G. Kim, S.-H. Choi, W.-B. Lee, G.M. Jeong, J. Koh, S. Lee, B. Kuh, J.-S. Park, Highly robust atomic layer deposition-indium gallium zinc oxide thin-film transistors with hybrid gate insulator fabricated via two-step atomic layer process for high-density integrated all-oxide vertical complementary metal-oxide-semiconductor applications, Small Struct. 5 (2024) 2300375, https://doi.org/10.1002/sstr.202300375.

[40] A. Marroun, N.A. Touhami, T.-E.-E. Hamadi, M.E. Bakkali, High-performance indium–gallium–zinc oxide thin-film transistors based on anodic aluminum oxide, Procedia Manuf. 32 (2019) 729–733, https://doi.org/10.1016/j.promfg.2019.02.278.

[41] S.D. Ponja, S. Sathasivam, I.P. Parkin, C.J. Carmalt, Highly conductive and transparent gallium doped zinc oxide thin films via chemical vapor deposition, Sci. Rep. 10 (2020) 638, https://doi.org/10.1038/s41598-020-57532-7.

[42] A.N. Løvik, E. Restrepo, D.B. Müller, Byproduct metal availability constrained by dynamics of carrier metal cycle: the gallium-aluminum example, Environ. Sci. Technol. 50 (2016) 8453–8461, https://doi.org/10.1021/acs.est.6b02396.

[43] S. Tougaard, Universality classes of inelastic electron scattering cross-sections, Surf. Interf. Anal. 25 (1997) 137.

[44] C.D. Wagner, Sensitivity factors for XPS analysis of surface atoms, J. Electron Spectr. Rel. Phenom. 32 (1983) 99–102.

[45] C.D. Wagner, A.V. Naumkin, A. Kraut-Vass, J.W. Allison, C.J. Powell, J.R. Rumble, NIST Standard Reference Database 20, Version 3.4 (web version) (http:/srdata.nist.gov/xps/) 2003.

[46] G. Beamson, D. Briggs, High-resolution XPS of organic polymers - the scienta ESCA300 database, Wiley (1992). Appendices 3.1 and 3.2.

[47] Y. Hu, L.C.M. Castro, E. Drouin, J. Florek, H. Kählig, D. Larivière, F. Kleitz, F.-G. Fontaine, Size-selective separation of rare earth elements using functionalized mesoporous silica materials, ACS Appl. Mater. Interfaces 11 (2019) 23681–23691, https://doi.org/10.1021/acsami.9b04183.

[48] I. Protsak, Y.M. Morozov, W. Dong, Z.-C. Le, D. Zhang, I.M. Henderson, A ^{29}Si, ^{1}H and ^{13}C solid-state NMR study on the surface species of various depolymerized organosiloxanes at silica surface, Nanoscale Res. Lett. 14 (2019) 160, https://doi.org/10.1186/s11671-019-2982-2.

[49] I. Protsak, I.M. Henderson, V. Tertykh, W. Dong, Z.-C. Le, Cleavage of organosiloxanes with dimethyl carbonate: a mild approach to graft-to-surface modification, Langmuir 34 (2018) 9719–9730, https://doi.org/10.1021/acs.langmuir.8b01580.

[50] I.S. Protsak, Y.M. Morozov, D. Zhang, V.M. Gun'ko, Surface chemistry of nanohybrids with fumed silica functionalized by polydimethylsiloxane/dimethyl carbonate studied using ^{1}H, ^{13}C, and ^{29}Si solid-state NMR spectroscopy, Molecules 26 (2021) 5974, https://doi.org/10.3390/molecules26195974.

[51] S.A. Wood, I.M. Samson, The aqueous geochemistry of gallium, germanium, indium, and scandium, Ore Geol. Rev. 28 (2006) 57–102, https://doi.org/10.1016/j.oregeorev.2003.06.002.

[52] I.S. Protsak, S. Champet, C.Y. Chiang, W. Zhou, S.R. Popuri, J. Willem, G. Bos, D. K. Misra, Y.M. Morozov, D.H. Gregory, Toward new thermoelectrics: tin selenide/modified graphene oxide nanocomposites, ACS Omega 4 (2019) 6010–6019, https://doi.org/10.1021/acsomega.8b03146.

[53] H. Zhang, X. Peng, G. Shi, W. Yan, M. Liang, Y. Chen, Z. Heng, H. Zou, Uniform macroporous amidoximated polyacrylonitrile monoliths for gallium recovery from bayer liquor, J. Appl. Polym. Sci. 138 (2021) 49764, https://doi.org/10.1002/app.49764.

[54] F. Zhao, Y. Zou, X. Lv, H. Liang, Q. Jia, W. Ning, Synthesis of $CoFe_2O_4$–zeolite materials and application to the adsorption of gallium and indium, J. Chem. Eng. Data 60 (2015) 338–1344, https://doi.org/10.1021/je501039u.

[55] M.O. Onizhuk, A.V. Panteleimonov, Y.V. Kholin, V.V. Ivanov, Dissociation constants of silanol groups of silic acids: quantum chemical estimations, J. Struct. Chem. 59 (2018) 261–271, https://doi.org/10.1134/S0022476618020026.

[56] M. Pfeiffer-Laplaud, D. Costa, F. Tielens, M.-P. Gaigeot, M. Sulpizi, Bimodal acidity at the amorphous silica/water interface, J. Phys. Chem. C 119 (2015) 27354–27362, https://doi.org/10.1021/acs.jpcc.5b02854.

[57] Z. Zhang, H. Zhang, Y. Hu, X. Yang, S. Yao, Novel surface molecularly imprinted material modified multi-walled carbon nanotubes as solid-phase extraction sorbent for selective extraction gallium ion from fly ash, Talanta 82 (2010) 304–311, https://doi.org/10.1016/j.talanta.2010.04.038.

[58] Y. Lu, L. Huang, Y. Guo, X. Yang, Theoretical insights into origin of graphene oxide acidity and relating behavior of oxygen-containing groups in water, Carbon 183 (2021) 355–361, https://doi.org/10.1016/j.carbon.2021.07.026.

[59] WebElements, https://www.webelements.com (last accessed 15th July 2024).

[60] C. Jeon, J.-H. Cha, J.-Y. Choi, Adsorption and recovery characteristics of phosphorylated sawdust bead for indium (III) in industrial wastewater, J. Ind. Eng. Chem. 27 (2015) 201–206, https://doi.org/10.1016/j.jiec.2014.12.036.
[61] N.-S. Kwak, Y. Baek, T.S. Hwang, The synthesis of poly(vinylphosphonic acid-co-methacrylic acid) microbeads by suspension polymerization and the characterization of their indium adsorption properties, J. Hazard. Mater. 203–204 (2012) 213–220, https://doi.org/10.1016/j.jhazmat.2011.12.020.
[62] W. Zeng, L. Xu, Q. Wang, C. Chen, M. Fu, Adsorption of indium (III) ions from an acidic solution by using UiO-66, Metals 12 (2022) 579, https://doi.org/10.3390/met12040579.
[63] J. Roosen, S. Mullens, K. Binnemans, Chemical immobilization of 8-hydroxyquinoline and 8-hydroxyquinaldine on chitosan-silica adsorbent materials for the selective recovery of gallium from bayer liquor, Hydrometall. 171 (2017) 275–284, https://doi.org/10.1016/j.hydromet.2017.05.026.
[64] Y. Hu, E. Drouin, D. Larivière, F. Kleitz, F.-G. Fontaine, Highly efficient and selective recovery of rare earth elements using mesoporous silica functionalized by preorganized chelating ligands, ACS Appl. Mater. Interfaces 9 (2017) 38584–38593, https://doi.org/10.1021/acsami.7b12589.
[65] J.-P. Simonin, On the comparison of pseudo-first order and pseudo-second order rate laws in the modeling of adsorption kinetics, Chem. Eng. J. 300 (2016) 254–263, https://doi.org/10.1016/j.cej.2016.04.079.
[66] M.A. Hubbe, S. Azizian, S. Douven, Implications of apparent pseudo-second-order adsorption kinetics onto cellulosic materials: a review, Bio. Resources 14 (2019) 7582–7626, https://doi.org/10.15376/biores.14.3.7582-7626.
[67] S. Gu, T. Tominaka, G. Dodbiba, T. Fujita, Recovery of indium and gallium from spent IGZO targets by leaching and solvent extraction, J. Chem. Eng. Jpn. 51 (2018) 675–682, https://doi.org/10.1252/jcej.17we298.
[68] Y. Wang, L. Zhu, Y. Song, Z. Lou, W. Shan, Y. Xiong, Novel chitosan-based ion imprinted bio-adsorbent for enhanced adsorption of gallium (III) in acidic solution, J. Mol. Liq. 320 (2020) 114413, https://doi.org/10.1016/j.molliq.2020.114413.
[69] E.I. El-Shafey, Removal of Zn(II) and Hg(II) from aqueous solution on a carbonaceous sorbent chemically prepared from rice husk, J. Hazard. Mater. 175 (2010) 319–327, https://doi.org/10.1016/j.jhazmat.2009.10.006.
[70] Y. Li, Z. Liu, Q. Li, Z. Liu, L. Zeng, Recovery of indium from used indium-tin oxide (ITO) targets, Hydrometall. 105 (2011) 207–212, https://doi.org/10.1016/j.hydromet.2010.09.006.
[71] C.W. Bock, G.D. Markham, A.K. Katz, J.P. Glusker, The arrangement of first- and second-shell water molecules in trivalent aluminum complexes: results from density functional theory and structural crystallography, Inorg. Chem. 42 (2003) 1538–1548, https://doi.org/10.1021/ed070pa25.5.